



Supplementary Materials for

Stable inhibitory activity of regulatory T cells requires the transcription factor Helios

Hye-Jung Kim, R. Anthony Barnitz, Taras Kreslavsky, Flavian D. Brown, Howell Moffett, Madeleine E Lamieux, Yasemin Kaygusuz, Torsten Meissner, Tobias A. W. Holderried, Susan Chan, Philippe Kastner, W. Nicholas Haining, and Harvey Cantor*

Correspondence to: Harvey_Cantor@dfci.harvard.edu

This PDF file includes:

Materials and Methods
Figs. S1 to S22
Table S1

MATERIALS AND METHODS

Mice. C57BL/6J (B6), FoxP3.GFP transgenic, FoxP3^{YFP}-Cre, OT-II transgenic, RIP-mOVA transgenic, CD4^{-/-} and CD8^{-/-} mice were obtained from the Jackson Laboratory (Bar Harbor ME). *Rag2*^{-/-}, *Rag2*^{-/-} γ *c*^{-/-}, *Rag2*^{-/-}*Prf1*^{-/-}, *K^b*^{-/-}*D^b*^{-/-} and CD45.1⁺ C57BL/6 were obtained from Taconic Farms. Helios-deficient (Helios^{-/-}) mice contain a global deletion of Helios and were generated as described (5); Helios^{+/+} (Helios WT) littermates are used as controls in experiments described here. Helios^{fl/fl}, Helios^{fl/fl}/CD4-Cre, and HY-TCR knock-in mice have been described (4, 24). Helios^{fl/fl}.FoxP3^{YFP}-Cre mice were generated by crossing Helios^{fl/fl} mice to FoxP3^{YFP}-Cre mice and are designated Helios^{fl/fl}.FoxP3-Cre (1). All mice were housed in specific pathogen-free conditions in the animal facilities at the Dana Farber Cancer Institute. All experiments were performed in compliance with federal laws and institutional guidelines as approved by DFCl's Animal Care and Use Committee.

Antibodies, flow cytometry. Fluorescence dye labeled Abs specific for CD3 (145-2C11), CD4 (L3T4), CD8 (53-6.7), TCR (H57-597), B220 (RA3-6B2), CD44 (IM7), CD62L (MEL-14), Fas (15A7), IgM (II/41), PD-1 (J43), CXCR5 (2G8), CD122 (TM- β 1), Ly49 (14B11), CD69 (H1.2F3), CD11b (M1/70), Gr-1 (RB6-8C5), CD45.1 (A20), HY-TCR (T3.70), V β 5 (MR9-4), CD45.1 (A20), Helios (22F6), FoxP3 (NRRF-30), CD73 (TY/11.8), FR4 (12A5), Lag3 (C9B7W), TIM-3 (RMT3-23), CD127 (A7R34), p-STAT5 (D47E7), IFN γ (XMG1.2), IL-17 (TC11-18H10), IL-4 (11B11), TNF α (MP6-XT22) and IL-10 (JES5-16E3) were purchased from BD, eBioscience, Biolegend and Cell Signaling. Intracellular staining for Helios and FoxP3 was performed using a FoxP3 staining buffer set (eBioscience). Intracellular staining for active Caspase-3 was performed using rabbit mAb (5A1E) followed by labeling with anti-rabbit AlexaFluor 647 Ab from Cell Signaling Technology after fixation of cells with Cytfix/Cytoperm buffer (BD Bioscience). Intracellular detection of IFN γ , IL-17 and TNF α was performed after restimulation of cells with 50 ng ml⁻¹ phorbol-12-myristate 13-acetate (Sigma) and 500 ng ml⁻¹ ionomycin (Sigma) and Golgistop (BD bioscience) for 4 hours. Stimulated cells were first stained for surface markers, fixed and permeabilized, and then stained with mAbs for different cytokines. For detection of p-STAT5, single-cell suspensions were prepared from spleens isolated from Helios^{+/+}, Helios^{-/-}, or Helios^{fl/fl}.FoxP3-Cre bone marrow chimeric mice. Five million splenocytes per condition were pre-treated with antibodies that block Fc receptors and then stained for surface antigens CD8a, TCR- β and CD25. These cell suspensions were washed in DMEM and subsequently serum-starved in DMEM for 45 min at 37°C. Cells remained unstimulated or stimulated with 100 U/ml IL-2 for 60 min and washed with PBS. Cells were fixed, permeabilized and stained for intercellular FoxP3 and p-STAT5 according to the flow cytometry protocol from Cell Signaling Technology.

Gene expression profiling. CD8 T cells were enriched from spleen cells of WT B6 mice using CD8 microbeads (Miltenyi) before staining with CD3, CD8, CD122 and Ly49. Ly49⁺ and Ly49⁻ CD8 cells were purified by cell sorting. RNA was prepared with the

RNeasy mini kit, according to manufacturer's instructions (Qiagen). RNA amplification, labeling and hybridization to MOA430 2.0 chips (Affymetrix) were performed at a Core Facility (Dana Farber Cancer Institute).

ChiP-Seq analysis. Purified CD4 (CD3⁺CD4⁺CD25⁺) and CD8 Treg (CD3⁺CD8⁺Ly49⁺) from spleen of WT B6 mice were activated *in vitro* by incubating with microbeads coated with anti-CD3 and anti CD28 Ab supplemented with IL-2 (CD4 Treg, 50 ng/ml) or IL-15 (CD8 Treg, 20 ng/ml) x5d. Activated CD4 and CD8 Treg were fixed for 10 min at 37°C with 1% formaldehyde. Cells were washed twice in ice-cold PBS and cell pellets were flash-frozen and stored at -80°C. For each Helios ChiP analysis in CD4 and CD8 Treg, 15×10⁶ – 20×10⁶ cells were used, and for each ChiP analysis of chromatin modification (trimethylation of histone H3 at Lys27 and acetylation of H3 at Lys27) 1.5×10⁶ cells were used. The following antibodies were used for ChiP: anti-Helios (G-20, Santa Cruz) (**Fig. S22**), anti-H3K27me3 (07-449, Millipore) and anti-H3K27ac (ab4729, Abcam). Preparation of ChiP immunocomplexes and DNA fragments, assays for high-throughput sequencing and ChiP-Seq informatics were performed according to protocols described previously (7).

Hematopoietic reconstitution. For generation of bone marrow chimeras, *Rag2*^{-/-} hosts received a lethal dose of radiation (900 rads) one day before BM cell transfer or two doses of 450 rads 4 hrs apart followed by reconstitution of BM cells. BM cells from donor mice were harvested by depleting NK1.1⁺, CD4⁺, CD8⁺ and TCR⁺ cells before 5×10⁶ cells were transferred (i.v.). For generation of Helios-sufficient and -deficient BM chimeras, BM cells from Helios^{+/+}, Helios^{-/-}, FoxP3^{YFP}-Cre, and Helios^{fl/fl}/Helios^{YFP}-Cre donors were transferred. For generation of mixed BM chimeric mice, 1:1 mixture of BM cells from CD4^{-/-} and Helios^{-/-}, CD8^{-/-} and Helios^{-/-}, Helios^{+/+} and Helios^{-/-}, Helios^{+/+} and Scurfy, Helios^{-/-} and Scurfy donors were injected, respectively. For analysis of negative selection and development of FoxP3⁺ CD4 Treg by self-reactive CD4 cells, lethally-irradiated WT B6 or RIP-mOVA Tg mice were reconstituted with BM cells from Helios^{+/+} or Helios^{-/-} OT-II Tg mice.

Immunohistochemistry. To assess immunopathology in multiple organs, mice were fixed with Bouin's solution before tissue sections were generated from paraffin-embedded tissues and stained with hematoxylin and eosin. For analysis of IgG deposition in kidney, 7 μm acetone-fixed frozen sections from kidney were stained with Alexa-Fluor[®] 488-conjugated anti-mouse IgG antibodies (Invitrogen). More than 10 tissue sections were examined for each experimental condition to verify reproducibility. Quantification of positively-stained areas was performed using ImageJ software and is depicted as pixel²/area.

LCMV-Armstrong infection. 2 month or 6 month old Helios WT or KO mice were infected i.p. with 2×10⁵ PFU LCMV-Armstrong. At day 30, mice were sacrificed and analyzed for lymphocyte profiles using spleen cells. Kidneys were harvested and cryosections were generated for analysis of IgG deposition.

Assessment of CD8 Treg suppressive activity in adoptive hosts. 2×10^6 B cells and 1×10^6 CD25 depleted CD4 cells were transferred into *Rag2*^{-/-} hosts along with 5×10^5 Ly49⁺ CD8 cells. For preparation of CD8 cells, spleen cells were harvested from mice that were immunized with 100 µg KLH in CFA and FACS-sorted by labeling with Abs for CD3, CD8, CD122 and Ly49. *Rag2*^{-/-} hosts were immunized with NP₁₉-KLH in CFA at day 0 and reimmunized with NP₁₉-KLH in IFA at day 10. Serum was prepared at day 10 and day 15 for measurement of primary and secondary responses, respectively.

Transfer model of colitis. Naïve CD4 cells (CD3⁺CD4⁺CD44^{lo}CD62L^{hi}, 4×10^5) sorted from Helios WT mice were transferred into *Rag2*^{-/-} hosts alone or in combination with Helios WT or Helios KO CD4 Treg (CD3⁺CD4⁺CD25⁺ or CD3⁺CD4⁺YFP⁺, 1×10^5). Two different Helios KO mouse strains (Helios^{-/-}, Helios^{fl/fl}.FoxP3^{YFP}-Cre) were tested. Mice were weighed weekly and monitored for signs of wasting disease. 6 wks after reconstitution, mice were sacrificed and spleen cells were analyzed for immune cell profiling; intestines were analyzed for histopathology.

CFSE labeling and transfer into *K^b*^{-/-}*D^b*^{-/-} mice. CD122⁺Ly49⁺, CD122⁺Ly49⁻ and CD122⁻ CD8 cells were FACS-sorted from WT B6 spleen cells. Cells were labeled with CFSE and transferred into *K^b*^{-/-}*D^b*^{-/-} mice that were depleted of NK1.1⁺ cells and sublethally (600 rads) irradiated 24 hrs before cell transfer. 5 days later, proliferation of CD8 cells was analyzed by measuring CFSE labeling intensity.

ELISA for antibodies. For detection of NP-specific antibodies, ELISA plates were coated with 0.5 µg/ml NP₄-BSA or 1 µg/ml NP₂₃-BSA for detection of high-affinity or total NP-specific antibodies (Biosearch Technologies). Serum harvested 14 days after immunization with NP₁₉-KLH in CFA and reimmunization with NP₁₉-KLH in IFA was used as a standard. 1:4000 dilution of this immune serum was defined as 100 units/ml. Antibodies with an IgG1 isotype were detected by incubating plates with biotinylated anti-mouse IgG1 followed by streptavidin-peroxidase. The amounts of ANA, anti-dsDNA, anti-SS/A, anti-SS/B were determined with ELISA kits from Alpha Diagnostic International. For detection of anti-thyroglobulin and anti-insulin Abs, porcine thyroglobulin (Sigma) and porcine insulin (Sigma) were used.

Retroviral transduction and cell culture

Gene expression analysis was performed using GFP or STAT5-CA expressing RV-pMIG (13). Viruses were produced from Plat-E cells transfected with GFP or STAT5-CA expressing RV pMIG as described (25). For retroviral transduction, CD4 Treg were purified from spleens of Helios^{+/+} and Helios^{-/-} mice by negative selection with magnetic beads (Treg expansion kit, Miltenyi Biotech) followed by sorting (CD3⁺CD4⁺CD25⁺), before incubation in anti-CD3/CD28 coated plates supplemented with IL-2 (10 ng/ml). Transduction was performed 24h later by centrifugation (1200 rpm x90m at RT) of CD4 Treg and addition of retroviral supernatants, 8 µg/ml polybrene and IL-2 (10 ng/ml) followed by medium replacement (DMEM with 10% FCS supplemented with IL-2 [10

ng/ml]) after 72h incubation. GFP⁺ cells were sorted and plated in anti-CD3/CD28-coated 96 well plates in the presence of IL-2 (0-50 ng/ml) and IL-4 (20 ng/ml) x5d and expression of FoxP3 and IFN γ production by CD4 Treg was measured by FACS.

Statistical analyses. Statistical significance was calculated according to Wilcoxon–Mann–Whitney rank sum test for comparison of two conditions; Kruskal–Wallis test was performed for comparison of more than two conditions. A *P* value of <0.05 was considered to be statistically significant (*= <0.05, ** = <0.01, *** = <0.001).

Author contributions: H.-J.K. and H.C. designed research; H.-J.K., R.A.B., T.K., F.D.B., H.M., M.E.L., Y.K., T.M., T.A.W.H. performed research; H.-J.K., R.A.B., T.K., F.D.B., H.M., Y.K., T.M., T.A.W.H., S.C., P.K., W.N.H., and H.C. analyzed data; H.-J.K. and H.C. wrote the paper

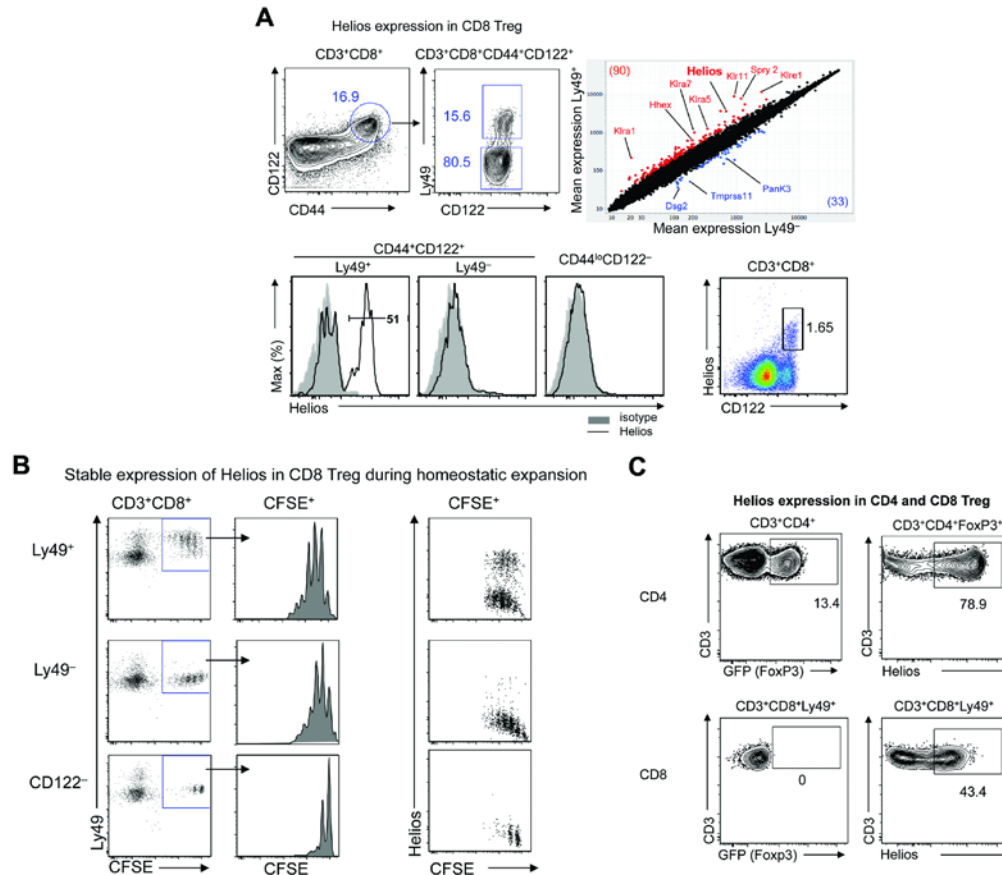


Fig. S1. Specific expression of Helios by CD44⁺CD122⁺Ly49⁺ CD8 Treg

A) cDNA from highly purified (>99%) CD44⁺CD122⁺Ly49⁺ and CD44⁺CD122⁺Ly49⁻ CD8 cells from spleen of B6 mice were subjected to DNA microarray analysis. 90 (red) and 33 (blue) genes were up- or down-regulated in CD44⁺CD122⁺Ly49⁺ CD8 cells by > 2 fold change. Expression of Helios by CD44⁺CD122⁺Ly49⁺ CD8 T cells, but not CD44⁺CD122⁺Ly49⁻ CD8 T cells was verified according to FACS analysis. Expression of Helios in the total CD8 T cell pool in spleen is shown at the bottom right. **B**) Stable expression of Helios in CD8 Treg during homeostatic expansion. *K^b-D^b-/-* mice were depleted of NK cells by injection of anti-NK1.1 Ab followed by sublethal (600 rads) irradiation. 24h later, CFSE labeled CD122⁺Ly49⁺, CD122⁺Ly49⁻ and CD122⁻ CD8 T cells were transferred intravenously. 5 days later, proliferation and expression of Helios by transferred CD8 cells was analyzed by FACS (n=4). In the FACS plot (left), CFSE negative cells are of host origin. Data are representative of at least 2 independent experiments. **C**) FoxP3-GFP reporter mice were analyzed for FoxP3 and Helios expression by FoxP3⁺ CD4 and Ly49⁺ CD8 T cells.

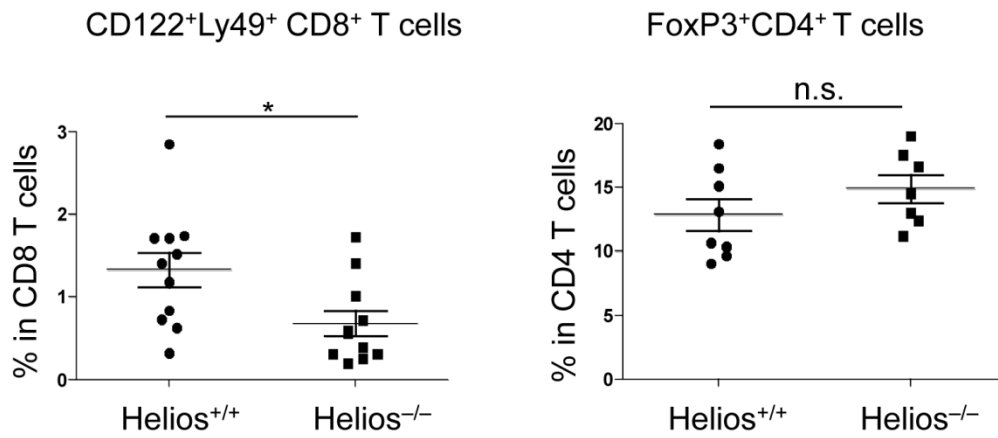


Fig. S2. Percentage of CD4 and CD8 Treg in Helios WT and KO mice.

The percentages of CD122⁺Ly49⁺ CD8 and FoxP3⁺CD4 cells within CD8 T and CD4 T cells, respectively, from spleens of Helios^{+/+} and Helios^{-/-} mice (6-8 wks old) are shown (n=7-11). Data are representative of at least three independent experiments. The mean \pm SEM is indicated. *P < 0.05 (Mann-Whitney test).

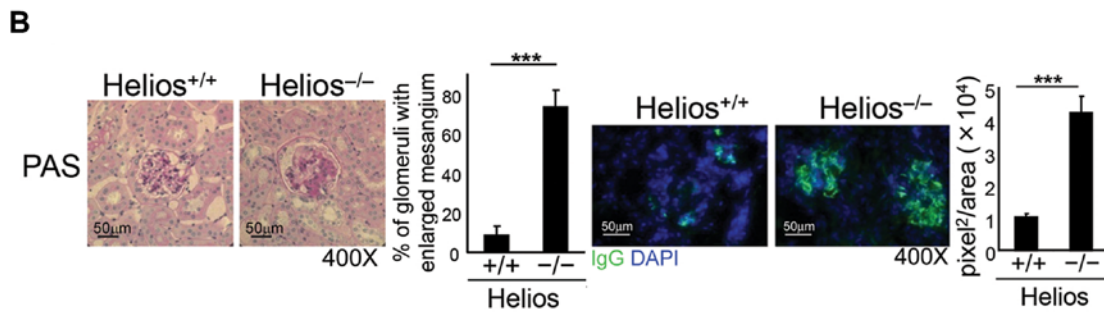
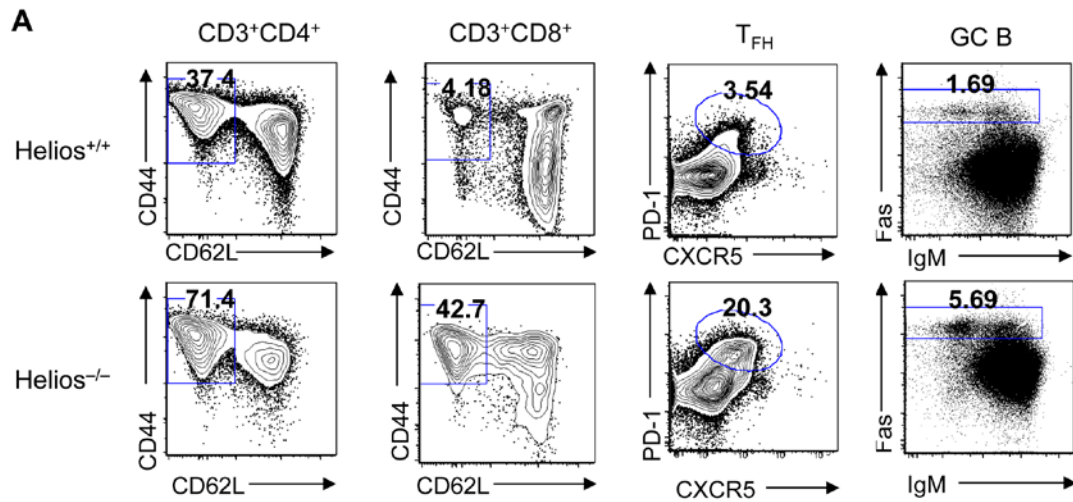


Fig. S3. Increased activated T cells, T_{FH} and GC B cells and kidney pathology in Helios^{-/-} mice.

A) Activated CD4 and CD8 T cells (CD44⁺CD62L^{lo}), T_{FH} (CD4⁺PD-1⁺CXCR5⁺), and GC B (B220⁺Fas⁺) cells in spleens from (5 mo old) Helios^{+/+} and Helios^{-/-} mice were compared (n=3-6). Representative data from three independent experiments. **B)** Kidney pathology of 7 mo old Helios^{+/+} and Helios^{-/-} mice assessed by PAS staining (400X) and IgG deposition (400X) in glomeruli is quantified (n=4). Representative data from three independent experiments. The mean ± SEM is indicated. ***P < 0.001 (Mann-Whitney test).

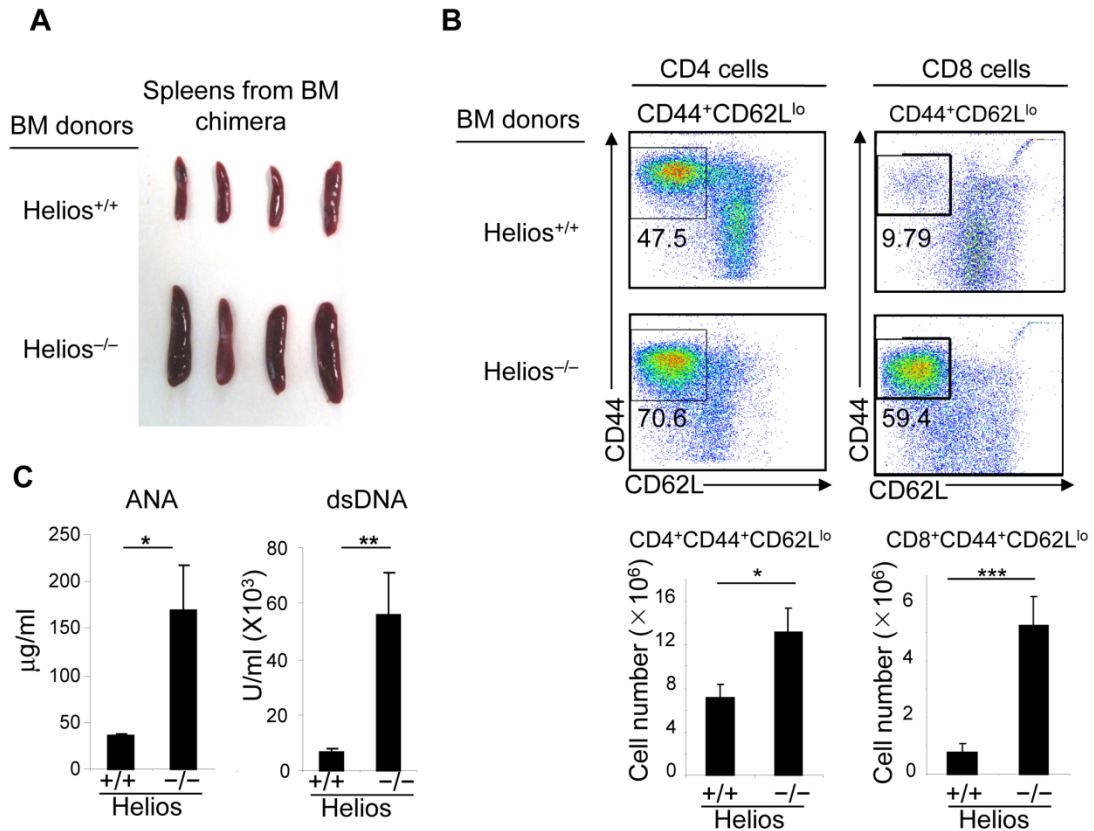


Fig. S4. Lymphocyte intrinsic effect of Helios deficiency on autoimmune development.

T and NK cell depleted BM cells from Helios^{+/+} and Helios^{-/-} mice were transferred to lethally irradiated (900 rads) Rag2^{-/-} hosts. 9 weeks later, mice were analyzed for immune phenotype. **A**) Spleens from BM chimera are shown. **B**) Flow cytometric analysis of CD44 and CD62L expression in spleen CD4⁺ and CD8⁺ T cells and **C**) autoantibodies from Rag2^{-/-} hosts reconstituted with Helios^{+/+} and Helios^{-/-} hematopoietic cells (n=4-5). All data are representative of at least three independent experiments. The mean \pm SEM is indicated. *P < 0.05, **P < 0.01 and ***P < 0.001 (Mann-Whitney test).

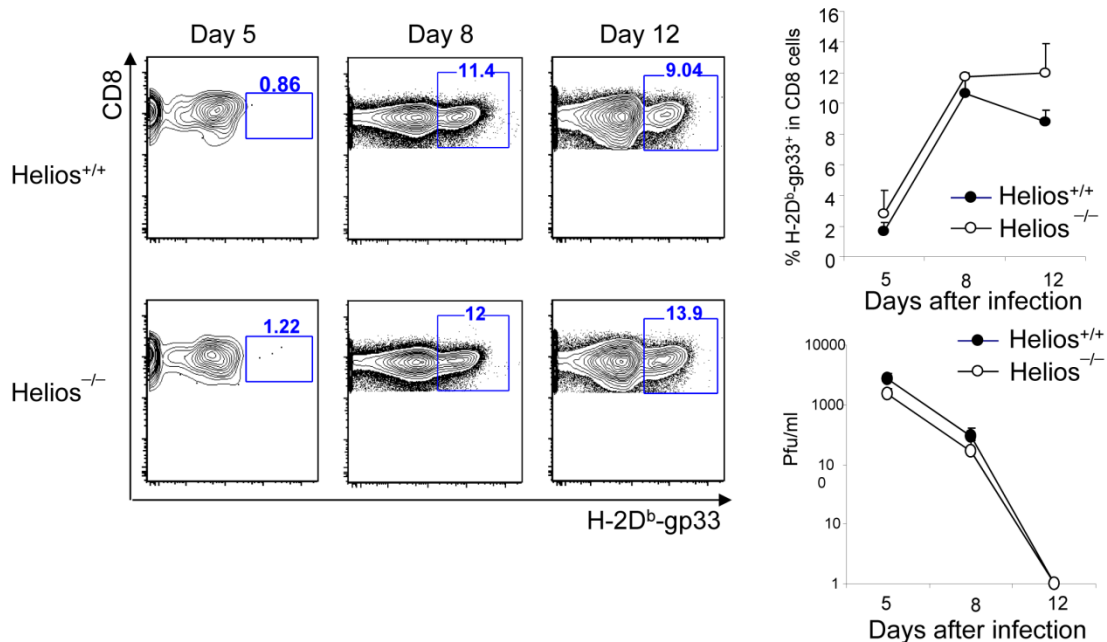


Fig. S5. Anti-viral immune responses in Helios WT and KO mice.

Analysis of LCMV-gp33 specific CD8 cells and virus titer after LCMV-Arm infection in Helios^{+/+} and Helios^{-/-} mice. 2 mo old Helios^{+/+} and Helios^{-/-} mice were infected i.p. with 2×10^5 pfu LCMV-Arm. Gp33 specific CD8⁺ T cells and virus titer in the blood were analyzed at day 5, 8 and 12 after infection (n=4). Data are representative of two independent experiments.

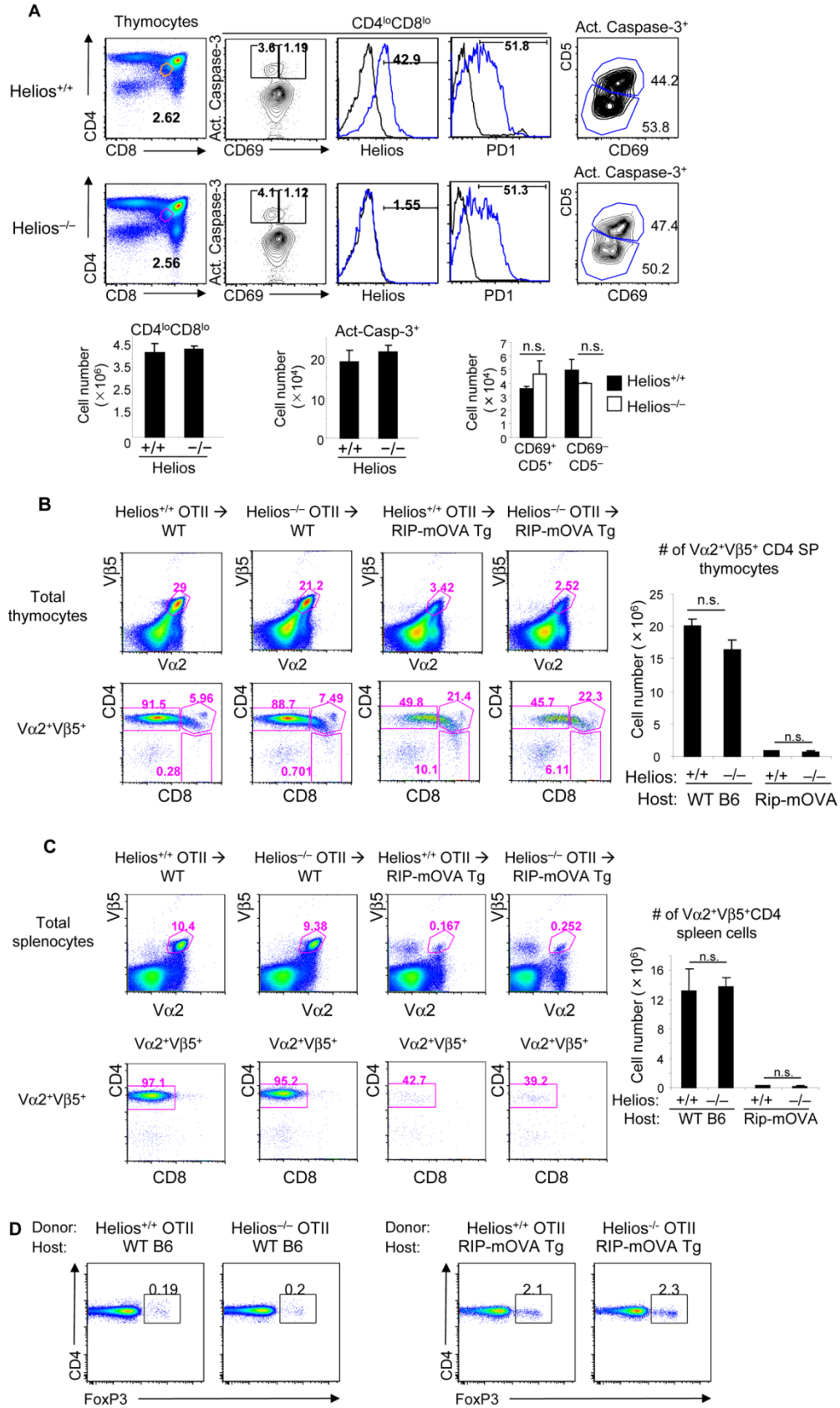


Fig. S6. Negative selection of selfreactive T cells and thymic generation of FoxP3⁺ CD4 Treg are not impaired by Helios deficiency.

A) Thymic negative selection is not defective in Helios^{-/-} mice. Flow cytometric analysis of Helios^{+/+} or Helios^{-/-} thymocytes for the percentage of CD4^{lo}CD8^{lo} subset and active Caspase-3, Helios (black: isotype, blue: Helios), PD-1 (black: isotype, blue: PD1) and CD5 and CD69 expression within apoptotic CD4^{lo}CD8^{lo} cells (n=4-5). **B)** Lethally irradiated WT B6 or RIP-mOVA transgenic mice were reconstituted with BM cells from Helios^{+/+} OT-II or Helios^{-/-} OT-II mice that were depleted of NK1.1⁺, TCR⁺, CD4⁺ and CD8⁺ cells. Development of OT-II cells (V_α2⁺V_β5⁺) was analyzed 8 weeks after reconstitution. Percentage and numbers of OT-II cells in total thymocytes (upper panel) and CD4 SP, DP and CD8 SP thymocytes within V_α2⁺V_β5⁺ thymocytes (lower panel) are shown (n=4). **C)** Percentage and numbers of V_α2⁺V_β5⁺ cells within total splenocytes and development of OT-II cells (CD4⁺) within total V_α2⁺V_β5⁺ splenocytes are shown (n=4). **D)** Helios deficiency does not impair thymic generation of self-reactive FoxP3⁺ CD4 Treg. Percentage of FoxP3⁺ CD4 cells in OT-II thymocytes in BM chimeras above was analyzed. Representative data from two independent experiments are shown (n=4). The mean ± SEM is indicated. n.s. (P > 0.05): not significant (Mann-Whitney test).

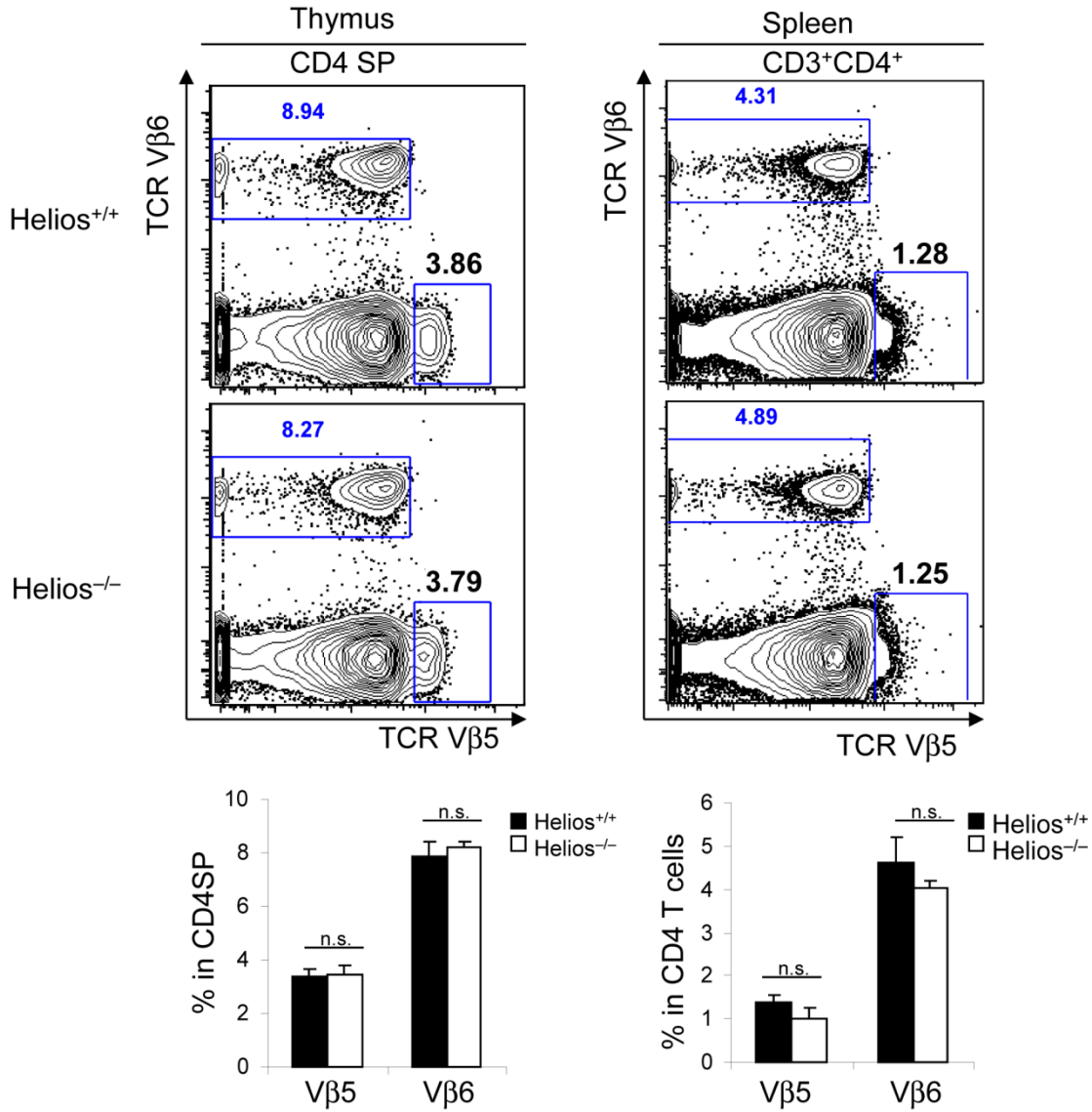


Fig. S7. . Helios deficiency does not impair MTV-mediated deletion of TCR V β 5⁺ CD4 cells.

Percentage of TCR V β 5⁺ CD4 cells in thymus and spleen was compared between Helios^{+/+} and Helios^{-/-} mice (haplotype: I-A^bI-E⁻). Percentage of TCR V β 6 serves as a reference (n=4-5). Data are representative of two independent experiments. The mean \pm SEM is indicated. n.s.: not significant (P > 0.05) (Mann-Whitney test).

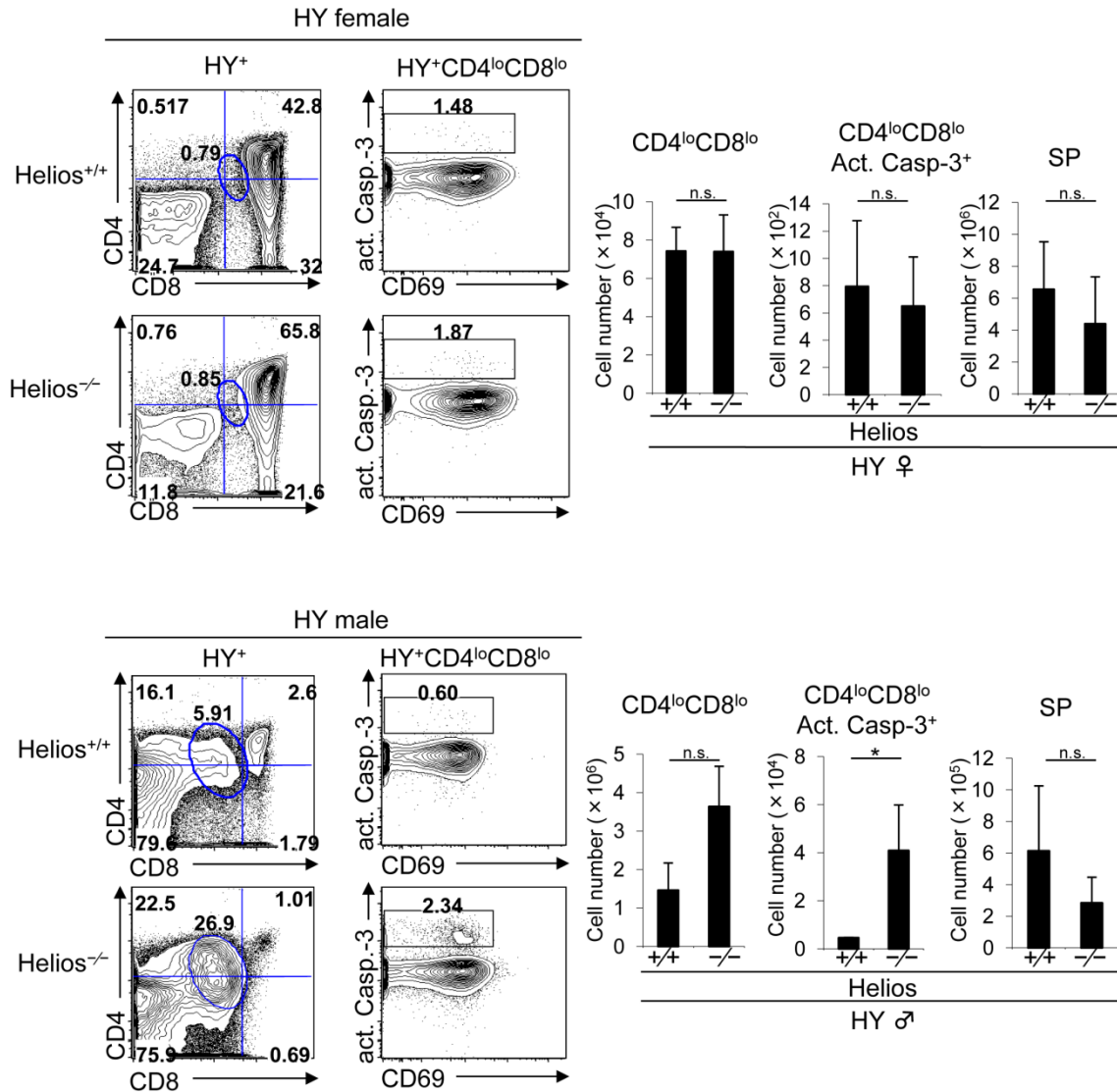


Fig. S8. Helios deficiency does not impair negative selection of selfreactive CD8 T cells.

HY TCR KI mice in Helios^{+/+} and Helios^{-/-} background were compared for the CD4^{lo}CD8^{lo} thymocytes undergoing apoptosis and development of HY⁺ SP T cells in female and male mice. Representative data from two independent experiments are shown (n=3). The mean ± SEM is indicated. *P < 0.05 and n.s.: not significant (P > 0.05) (Mann-Whitney test).

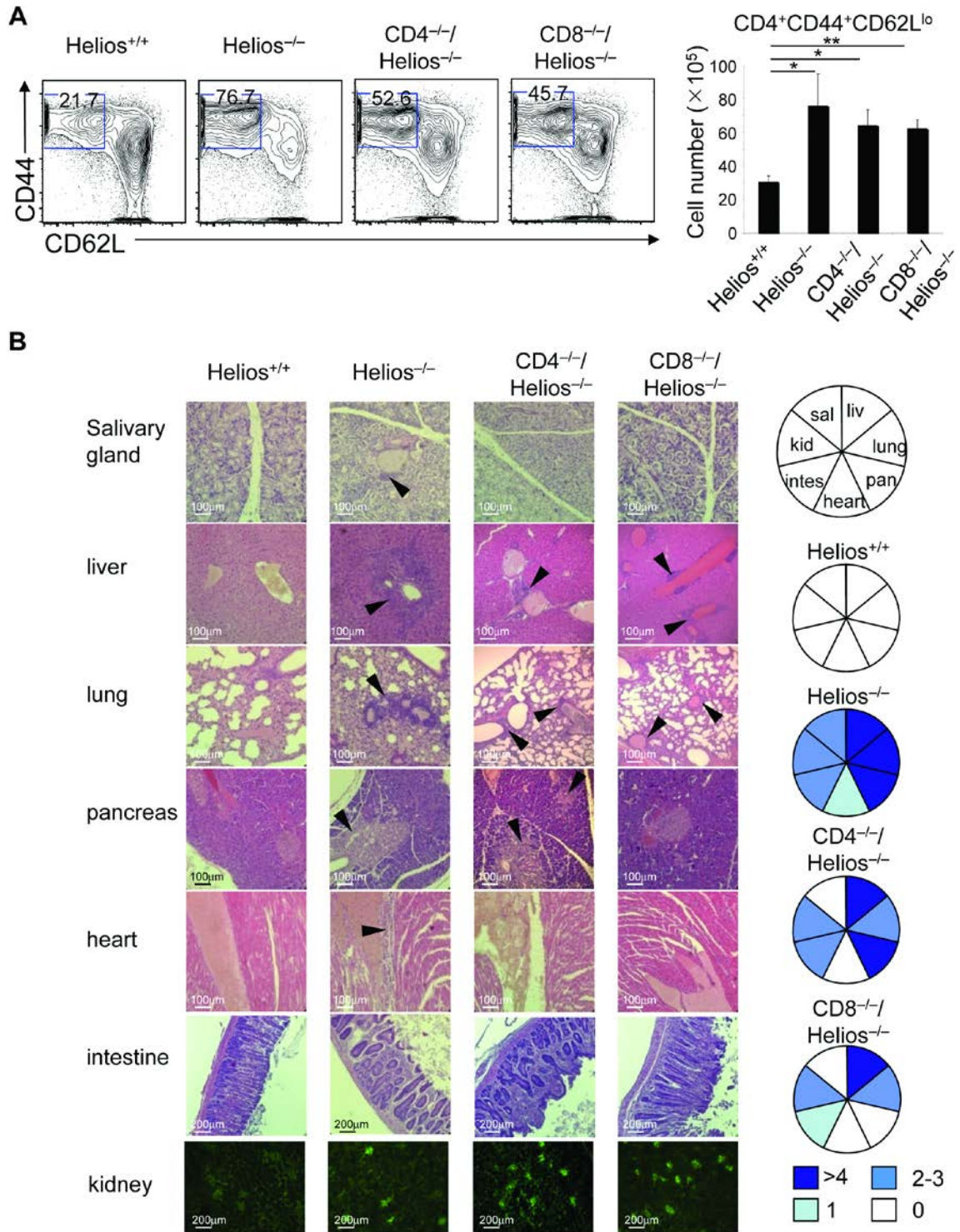


Fig. S9. Helios deficiency in both CD4 and CD8 T cells contributes to the perturbed immune homeostasis.

Lethally irradiated *Rag2*^{-/-} hosts were reconstituted with NK1.1⁺ and TCR⁺-depleted BM cells that were Helios^{+/+}, Helios^{-/-}, 1:1 ratio of CD4^{-/-} + Helios^{-/-}, or 1:1 ratio of CD8^{-/-} + Helios^{-/-} BM to generate mice containing lymphoid cells that were Helios sufficient, Helios-deficient, or mice with a selective Helios deficiency in either CD4 or CD8 T cells.

A) Flow cytometric plots for activated CD4 (CD44⁺CD62L^{lo}CD4⁺) cells and numbers in spleen are shown (n=5). Representative data from two independent experiments are shown. The mean \pm SEM is indicated. *P < 0.05 and **P < 0.01 (Mann-Whitney test). **B)** Analysis of immune cell infiltration into various organs from *Rag2*^{-/-} mice reconstituted with hematopoietic precursors described in A). Intensity of immune cell infiltration into peripheral organs was quantified by scoring tissue sections: >4 (most severe), 2-3 (severe), 1 (mild) and 0 (none) (n=5). Data representative of two independent experiments.

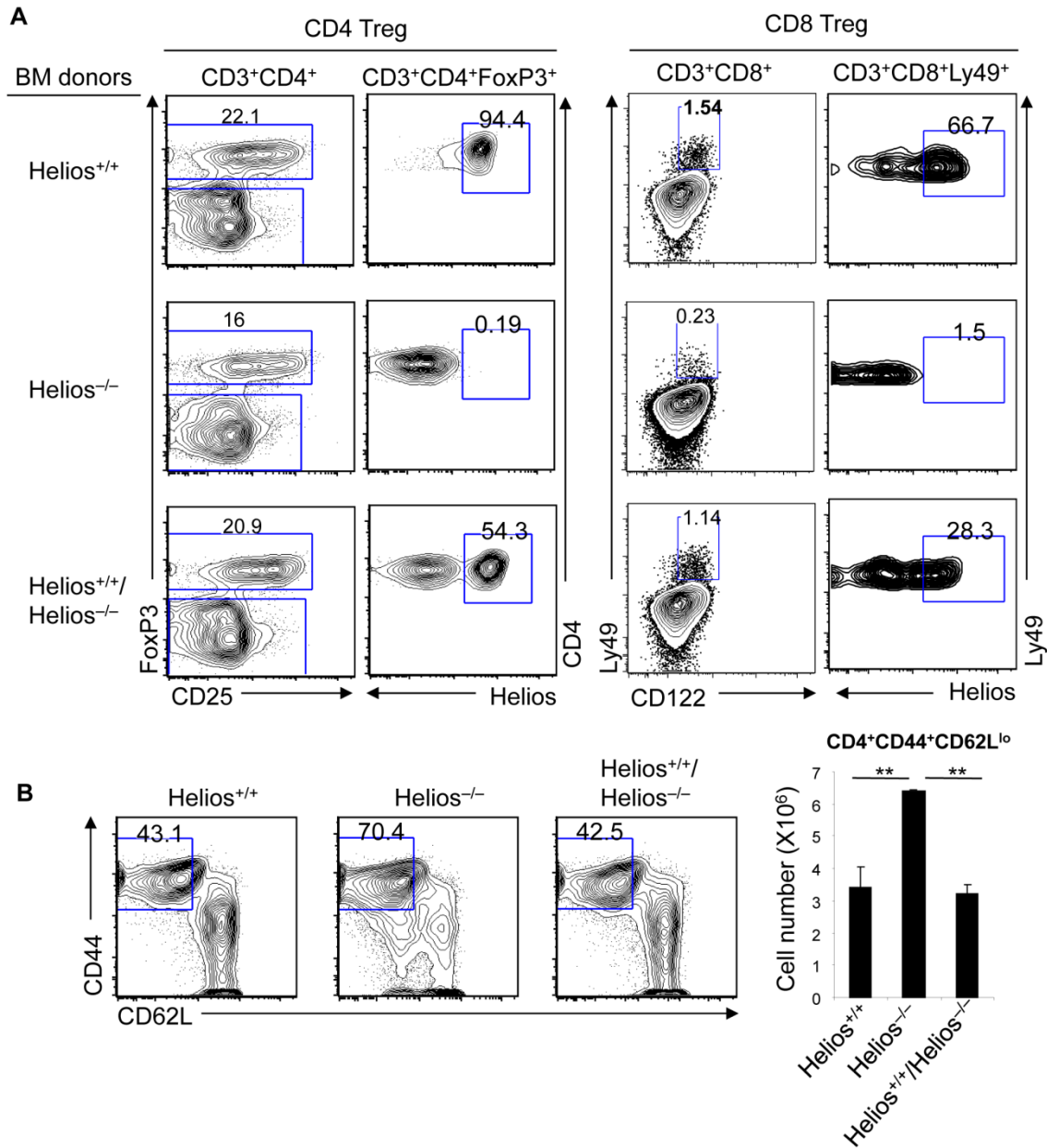


Fig. S10. Helios^{+/+} and Helios^{+/+}/Helios^{-/-} BM chimera show similar levels of CD4 T cell activation.

Lethally irradiated *Rag2*^{-/-} mice were reconstituted with hematopoietic progenitors from Helios^{+/+}, Helios^{-/-} and Helios^{+/+} + Helios^{-/-} (1:1) mice. **A)** Helios expression by FoxP3⁺ CD4 Treg and Ly49⁺ CD8 Treg were analyzed with spleen cells from each BM chimera. **B)** Percentage of activated CD4 cells were analyzed in these BM chimera. Histological analyses confirmed this finding (see Fig. 2D) (n=5). Data (A, B) representative of two independent experiments. The mean ± SEM is indicated. **P < 0.01 (Mann-Whitney test).

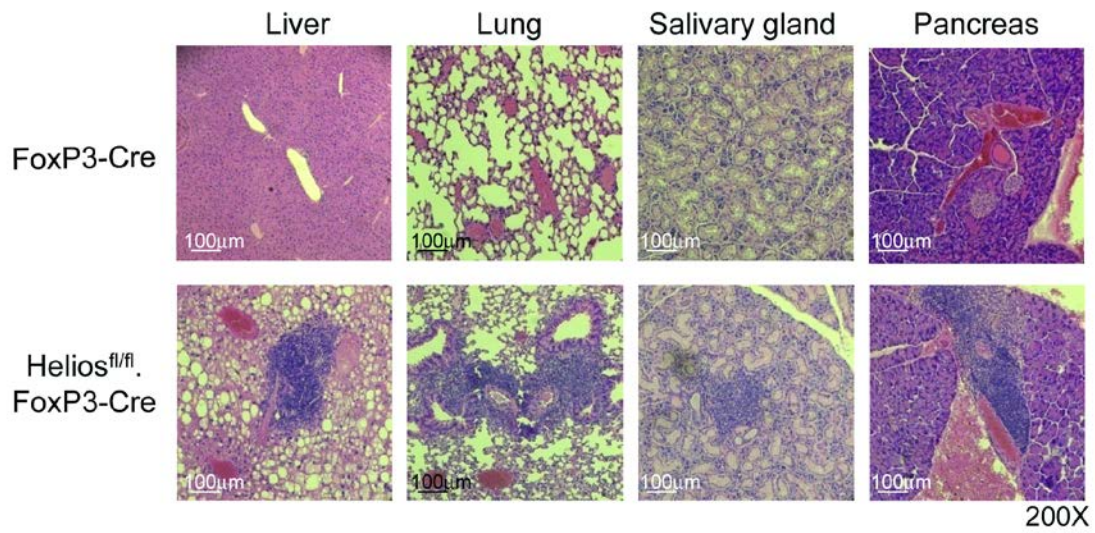


Fig. S11. Lymphoid infiltration into non-lymphoid tissues in Helios^{fl/fl}.FoxP3-Cre mice.

Microscopy (200X) of representative hematoxylin and eosin staining of liver, lung, salivary gland, pancreas from 6 mo old FoxP3-Cre and Helios^{fl/fl}.FoxP3-Cre mice. Data representative of two independent experiments.

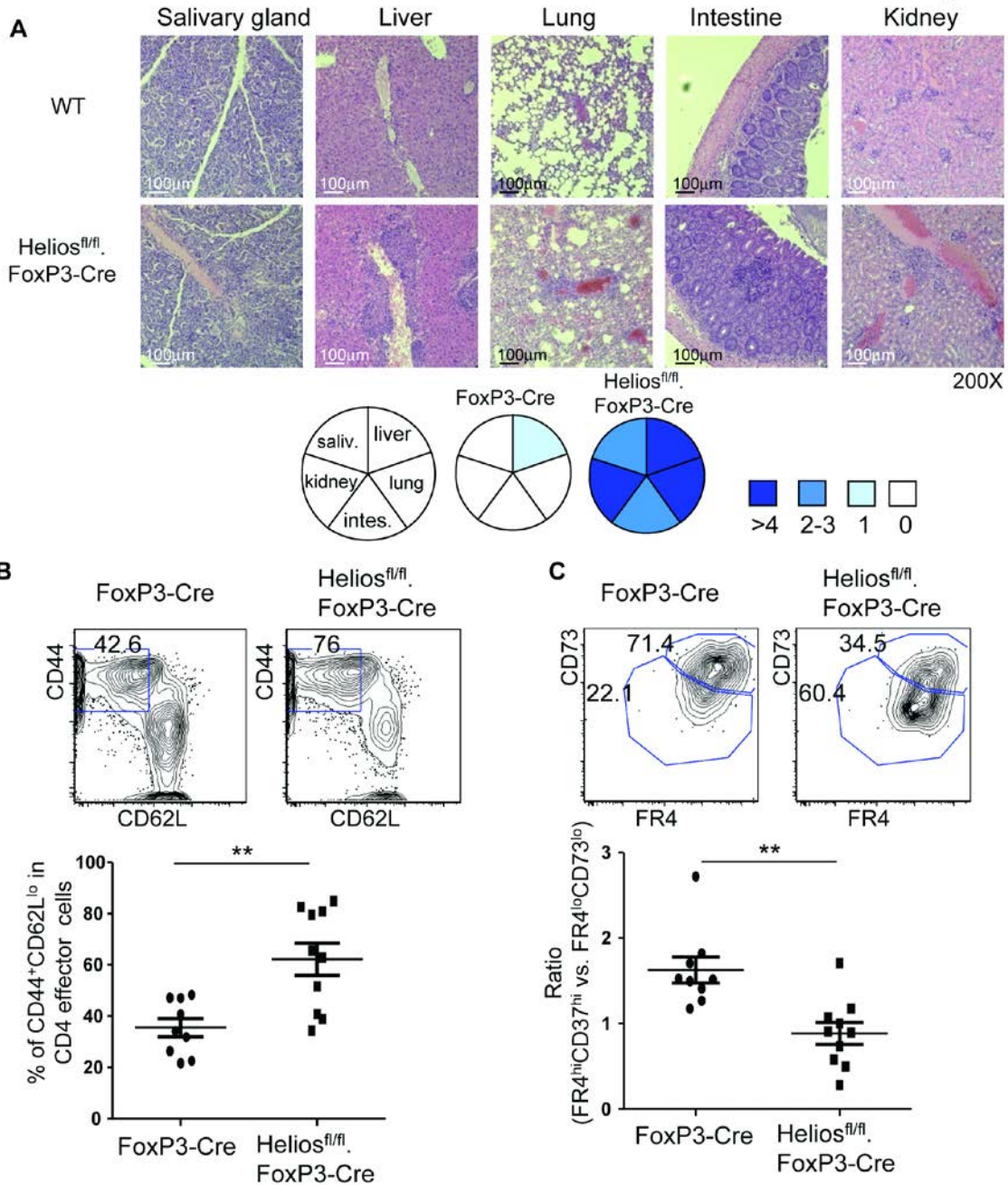


Fig. S12. Development of autoimmune disease in Helios^{fl/fl}.FoxP3-Cre BM chimeras.

NK1.1⁺, CD4⁺, CD8⁺ TCR⁺ depleted BM cells from WT (FoxP3-Cre) or Helios^{fl/fl}.FoxP3-Cre mice were transferred into lethally irradiated Rag2^{-/-} mice before analysis for signs of autoimmune disease 6 weeks after BM transfer. **A**) Immune cell infiltration into multiple organs was analyzed. **B**) Percentage of activated CD4 cells and **C**) expression of FR4 and CD73 by FoxP3⁺ CD4 T cells was analyzed with spleen cells from these BM chimeras (n=9-10). Data are representative of two independent experiments. The mean ± SEM is indicated. **P < 0.01 (Mann-Whitney test).

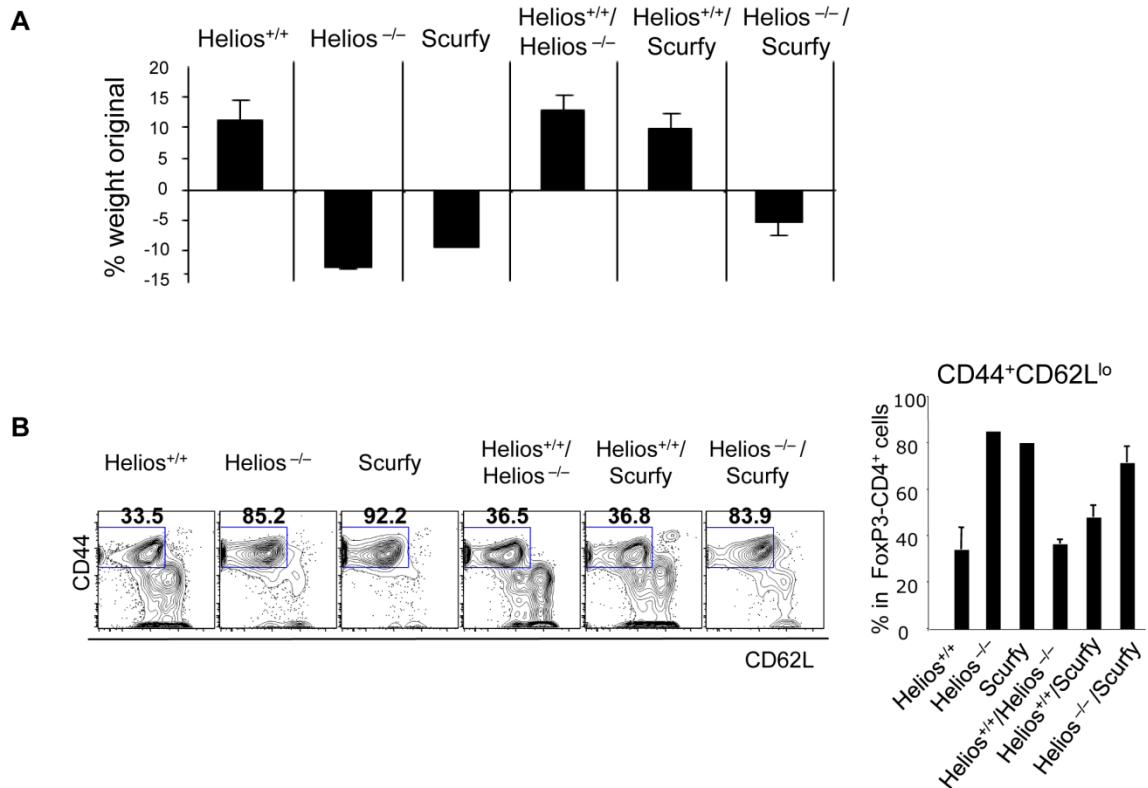


Fig. S13. Selective Helios deficiency in FoxP3⁺ cells contributes to the development of autoimmune disease.

Lethally irradiated *Rag2*^{-/-} mice were reconstituted with hematopoietic progenitors from Helios^{+/+}, Helios^{-/-}, Scurfy, Helios^{+/+} + Helios^{-/-} (1:1), Helios^{+/+} + Scurfy (1:1), and Helios^{-/-} + Scurfy (1:1) mice (n=4-6). **A**) The change of body weight was monitored. The percentage weight change 7 weeks after reconstitution is shown (n=4-6). **B**) Levels of activated CD4 cells are shown as percentage of CD44⁺CD62L^{lo}FoxP3⁺ cells within CD4 T cells (n=4-6). Data are representative of two independent experiments.

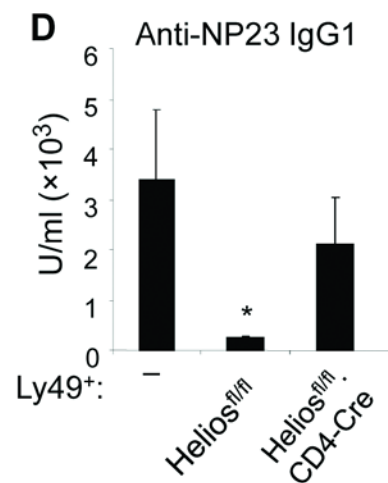
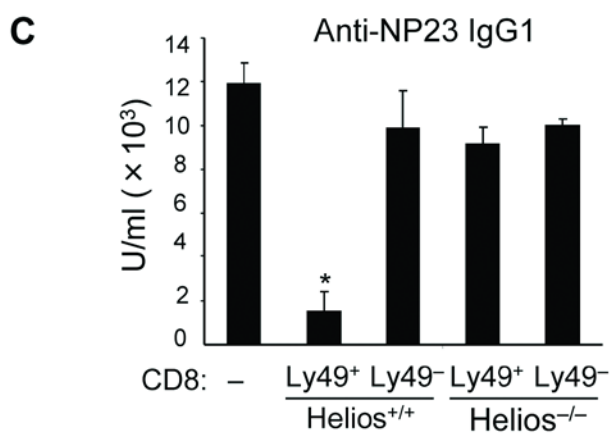
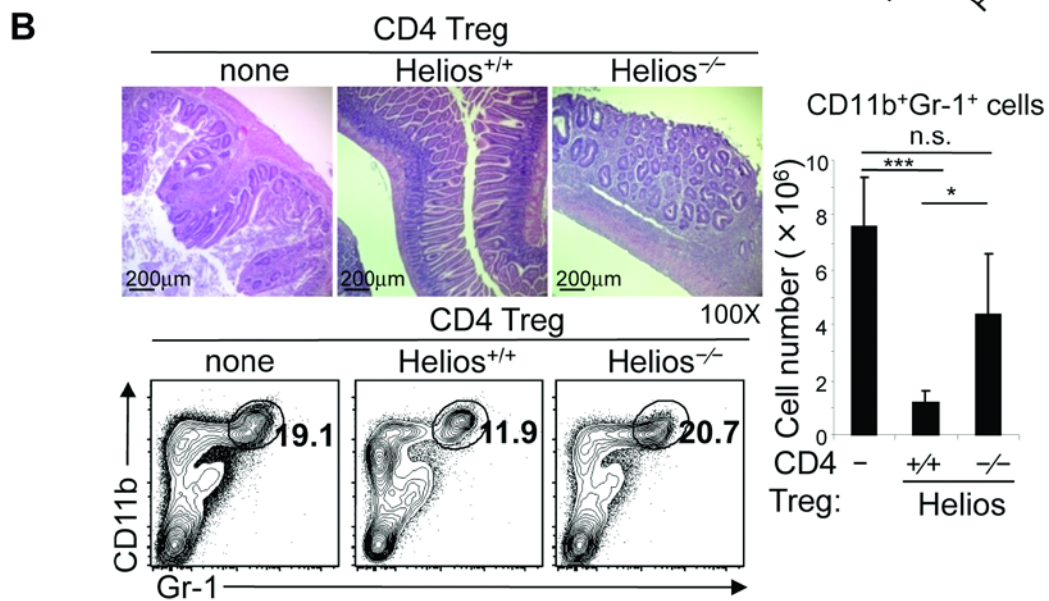
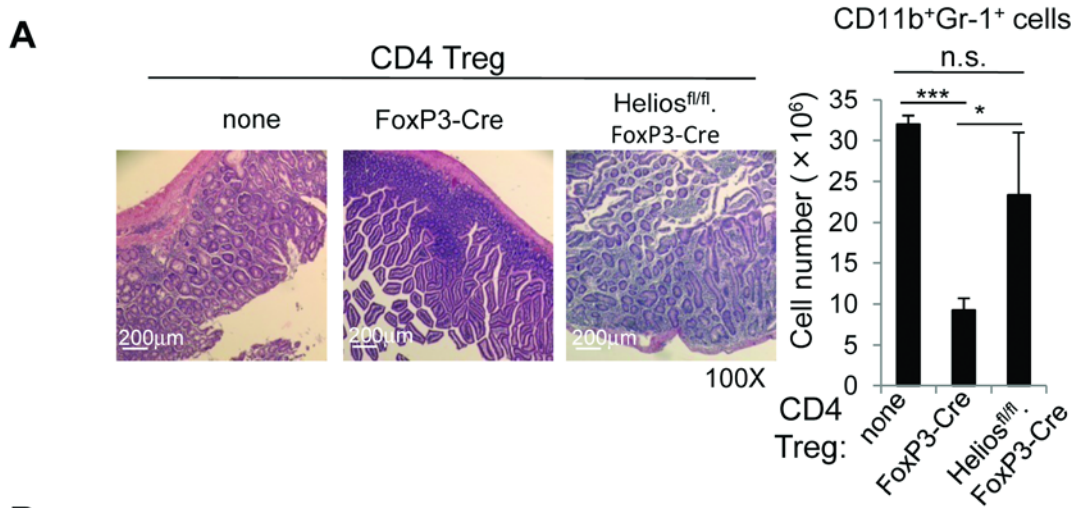


Fig. S14. . Defective inhibitory activity of Helios deficient CD4 and CD8 Treg.

A) *Rag2*^{-/-} hosts received sort-purified Teff cells (CD25⁻CD44^{lo}CD62L^{hi}, CD45.1) and CD4 Treg (CD3⁺CD4⁺YFP⁺) from spleens of FoxP3-Cre or Helios^{fl/fl}.FoxP3-Cre mice. Recipients were examined for microscopy of intestine pathology and number of CD11b⁺Gr-1⁺ cells in spleen (n=4). Representative data from two independent experiments. The mean ± SEM is indicated. *P < 0.05 and ***P < 0.001 (Kruskal-Wallis test). **B)** *Rag2*^{-/-} hosts received sort-purified CD4 T cells (Teff: CD25⁻CD44^{lo}CD62L^{hi}, CD4 Treg: CD3⁺CD4⁺CD25⁺) from spleens of defined donor mouse strains. Recipients were examined for microscopy of intestine pathology and number of CD11b⁺Gr-1⁺ cells in spleen (n=4). Representative data from three independent experiments. The mean ± SEM is indicated. *P < 0.05, and ***P < 0.001 (Kruskal-Wallis test). **C)** Defective suppressive function of Helios^{-/-} CD8 Treg. WT splenic B and CD25-depleted CD4 T cells were transferred into *Rag2*^{-/-} hosts along with Ly49⁺ or Ly49⁻ CD8 T cells from spleens of *Rag2*^{-/-} BM chimera reconstituted with Helios^{+/+} or Helios^{-/-} hematopoietic cells. *Rag2*^{-/-} adoptive hosts were immunized with NP₁₉-KLH in CFA at day 0 and reimmunized with NP₁₉-KLH in IFA at day 10. Secondary IgG1 response to NP is shown (n=3). Data shown are representative of two independent experiments. The mean ± SEM is indicated. *P < 0.05 (Kruskal-Wallis test). **D)** Suppressive activity of Ly49⁺ CD8 cells from Helios^{fl/fl} or Helios^{fl/fl}.CD4-Cre mice. Splenic B cells (1×10⁶) and CD25⁺ depleted WT CD4 cells (0.5 × 10⁶) were transferred into *Rag2*^{-/-}*Prf1*^{-/-} hosts along with FACS-purified Ly49⁺ CD8 cells (2.5 × 10⁵) from spleens of Helios^{fl/fl} or Helios^{fl/fl}.CD4-Cre mice. *Rag2*^{-/-}*Prf1*^{-/-} mice were immunized with NP₁₉-KLH in CFA, before reimmunization 10 days later with NP₁₉-KLH in IFA. Serum levels of IgG1 antibodies specific for NP23 were measured on day 18 (n=4-5). Representative data from two independent experiments. The mean ± SEM is indicated. *P < 0.05 (Kruskal-Wallis test).

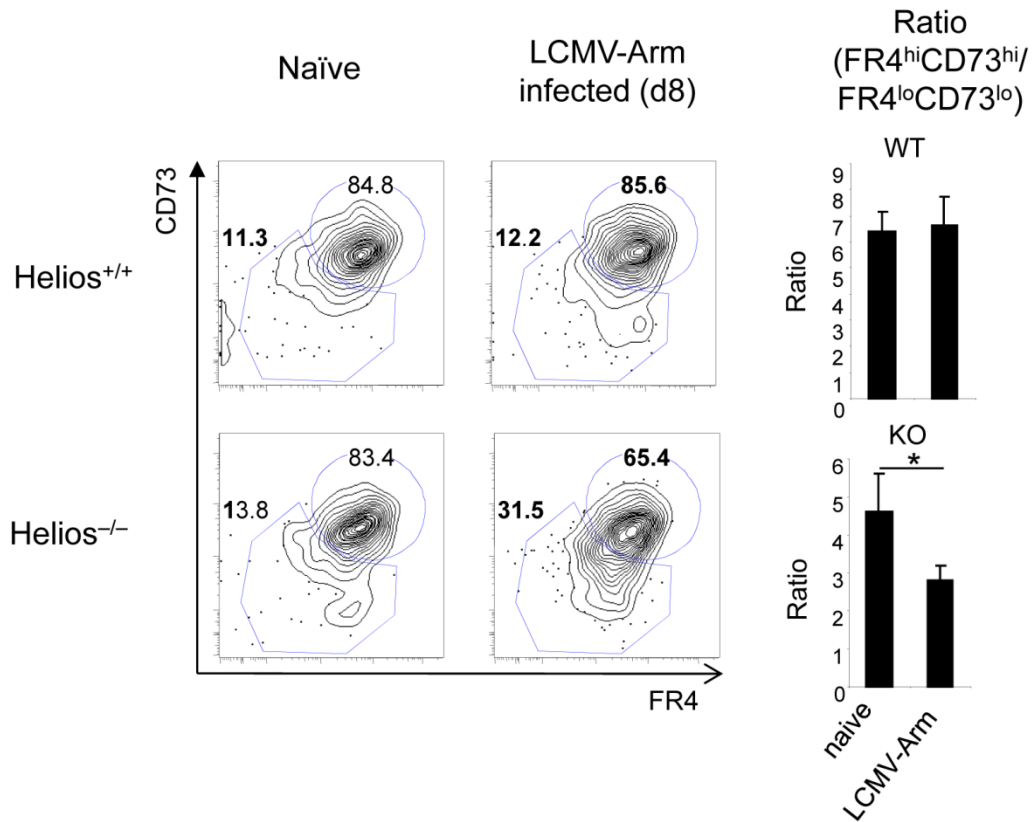


Fig. S15. Helios deficient CD4 Treg acquire non-energetic phenotype in the inflammatory environment.

Helios^{+/+} and Helios^{-/-} mice were infected i.p. with 2×10^5 pfu LCMV-Armstrong. At day 8 after infection, spleen cells were harvested and the surface phenotype of FoxP3⁺ CD4 Treg in spleen was analyzed (n=4). Data are representative of two independent experiments. The mean \pm SEM is indicated. *P < 0.05 (Mann-Whitney test).

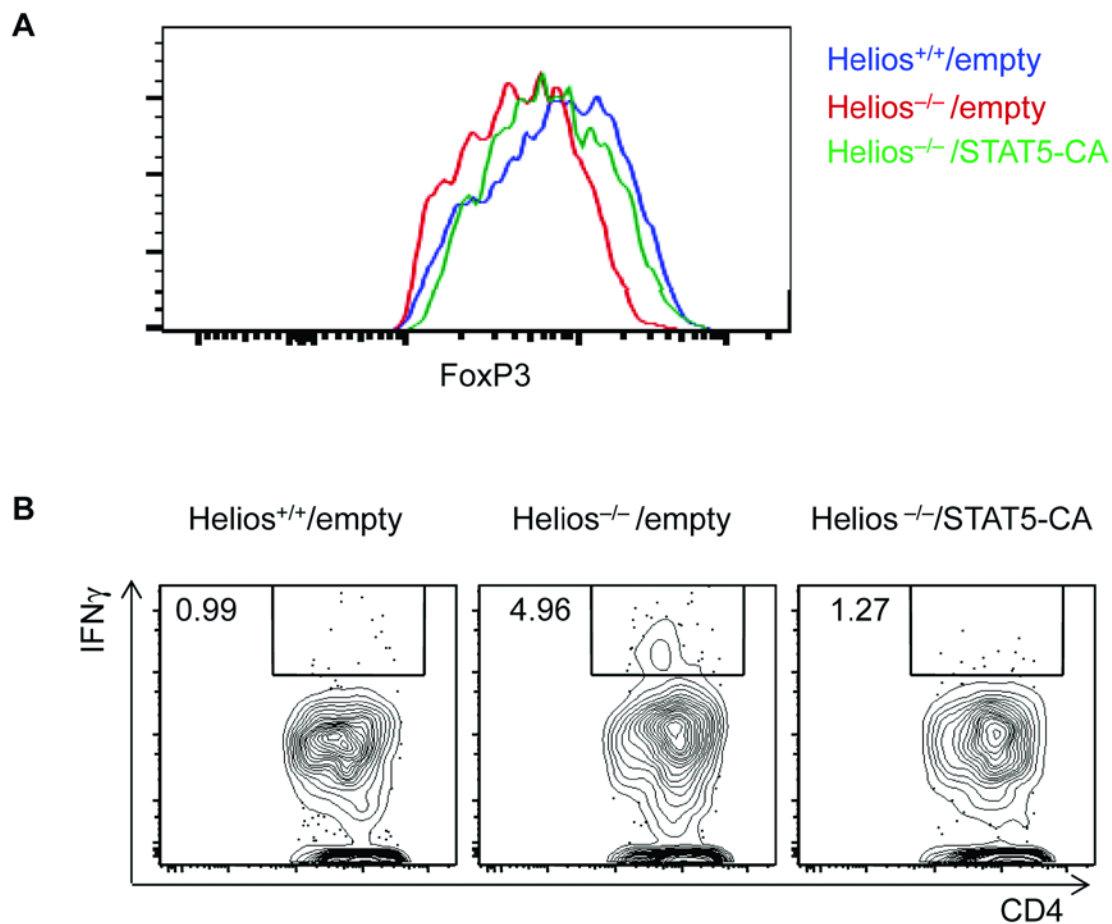


Fig. S16. Expression of STAT5-CA rescues impaired CD4 Treg phenotype of Helios^{-/-} CD4 Treg.

CD4 Treg from Helios^{+/+} and Helios^{-/-} mice were transduced with retrovirus expressing GFP or STAT5-CA/GFP, before stimulation with plate-coated anti-CD3/CD28 Abs in the presence of IL-2 (0-50 ng/ml; shown at 5 ng/ml) and IL-4 (20 ng/ml) before measurement of **A**) FoxP3 expression and **B**) expression of IFN γ 5 days later. Data are representative of two experiments.

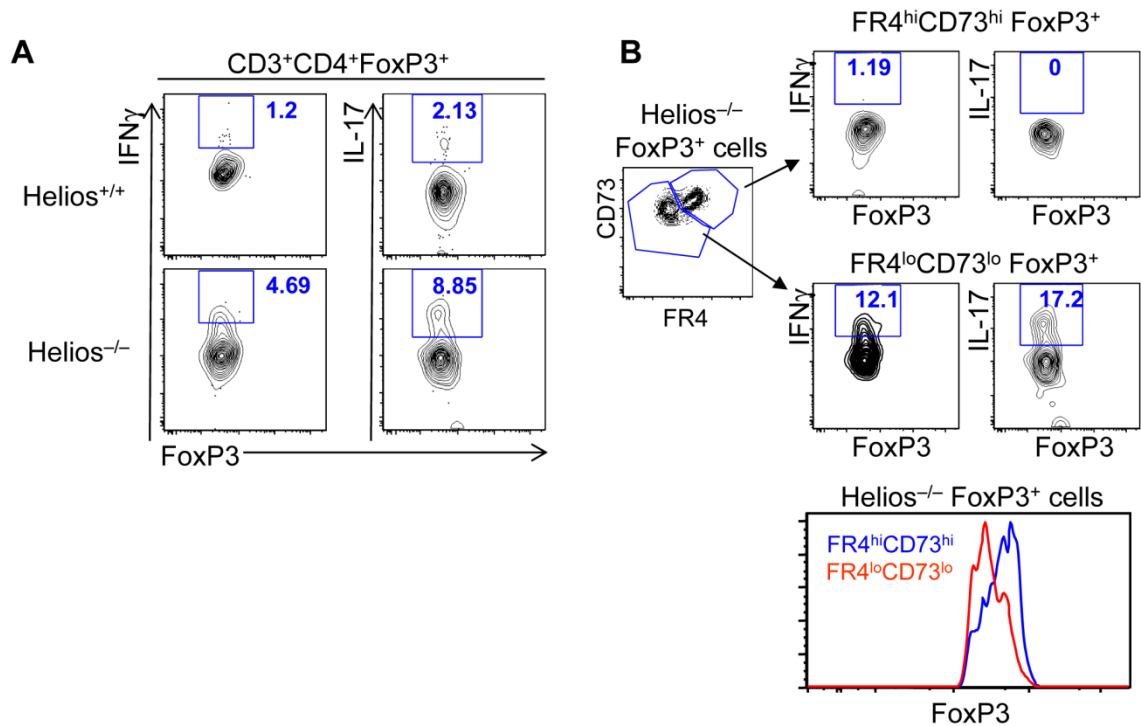


Fig. S17. Helios deficient CD4 Treg express effector cytokines.

A) Effector cytokine expression by Helios-deficient CD4 Treg isolated from spleens of *Rag2*^{-/-} hosts following colitis induction (see Fig. 2F). **B)** Expression of effector cytokines by Helios-deficient CD4 Treg is confined to FR4^{lo}CD73^{lo} subset. Helios^{-/-} CD4 Treg isolated from spleens of *Rag2*^{-/-} mice with progressive colitis were analyzed for IFN γ and IL-17 expression after *in vitro* stimulation with PMA and ionomycin based on FR4 and CD73 expression (FR4^{hi}CD73^{hi} and FR4^{lo}CD73^{lo}). Levels of FoxP3 expression by FR4^{hi}CD73^{hi} and FR4^{lo}CD73^{lo} cells in Helios^{-/-} CD4 Treg recovered from spleens of *Rag2*^{-/-} hosts are shown (lower panel). Representative FACS plots from three independent experiments are shown.

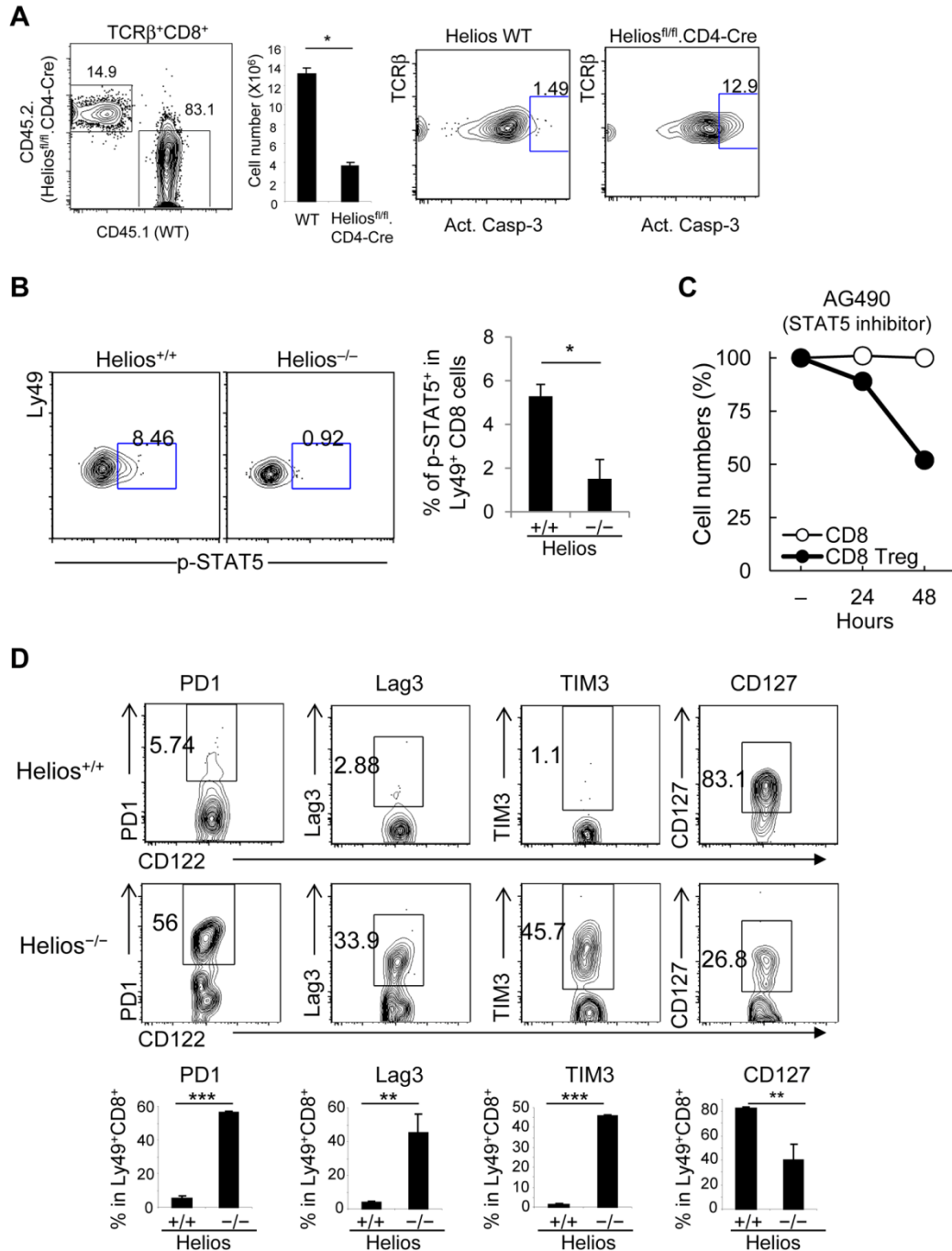


Fig. S18. Helios-dependent STAT5 activation and stabilization of CD8 Treg.
A) Ly49⁺ CD8 Treg from spleens of Helios WT (CD45.1⁺) and Helios KO (Helios^{fl/fl}/CD4-Cre, CD45.2⁺) mice were transferred into *Rag2*^{-/-}*Prf1*^{-/-} mice along with OT-II cells (V α 2⁺V β 5⁺) followed by immunization with OT-II peptides (10 μ g) in IFA. 5 days later, the percentage of Ly49⁺ CD8 cells from each origin and levels of apoptosis in spleens were analyzed (n=4-5). Representative data from two independent experiments are shown. The mean \pm SEM is indicated. *P < 0.05 (Mann-Whitney test). **B)** IL-2 responsiveness by Helios^{+/+} and Helios^{-/-} CD8 Treg. Helios^{+/+} and Helios^{-/-} mice were infected with LCMV-Arm (1 \times 10⁶ pfu). Two months later, spleen cells isolated from these mice were

stimulated with IL-2 (100 U/ml) *in vitro*. IL-2 responsiveness of Ly49⁺ CD8 cells was measured by levels of p-STAT5 expression by FACS. FACS plots show the proportion of p-STAT5⁺ cells within Ly49⁺ CD8 cells. Representative data from two independent experiments are shown (n=4-5). The mean \pm SEM is indicated. *P < 0.05 (Mann-Whitney test). **C**) Analysis of the impact of STAT5 inhibitor on conventional CD8 T cells and CD8 Treg. FACS-purified conventional memory-type CD8 cells (CD44^{hi}CD122⁺Ly49⁻) and CD8 Treg (CD44^{hi}CD122⁺Ly49⁺) were cultured in the presence of DMSO or AG490 (STAT5 inhibitor) and relative number of cells treated with AG490 compared to DMSO treated cells were analyzed. Data representative of 3 independent experiments are shown. **D**) Helios-deficient CD8 Treg acquire phenotypic characteristics of dysfunctional CD8 T cells during the rapid progression of autoimmunity. Lethally irradiated *Rag2*^{-/-} mice were reconstituted with hematopoietic precursors from Helios^{+/+} or Helios^{-/-} mice (n=4-6). At the time point of robust autoimmune progression (~8 wks after BM reconstitution), Ly49⁺ CD8 T cells from spleens of these mice were analyzed for expression of PD-1, Lag3, TIM3 and CD127. Representative data from two independent experiments are shown. The mean \pm SEM is indicated. *P < 0.05, **P < 0.01 and ***P < 0.001 (Mann-Whitney test).

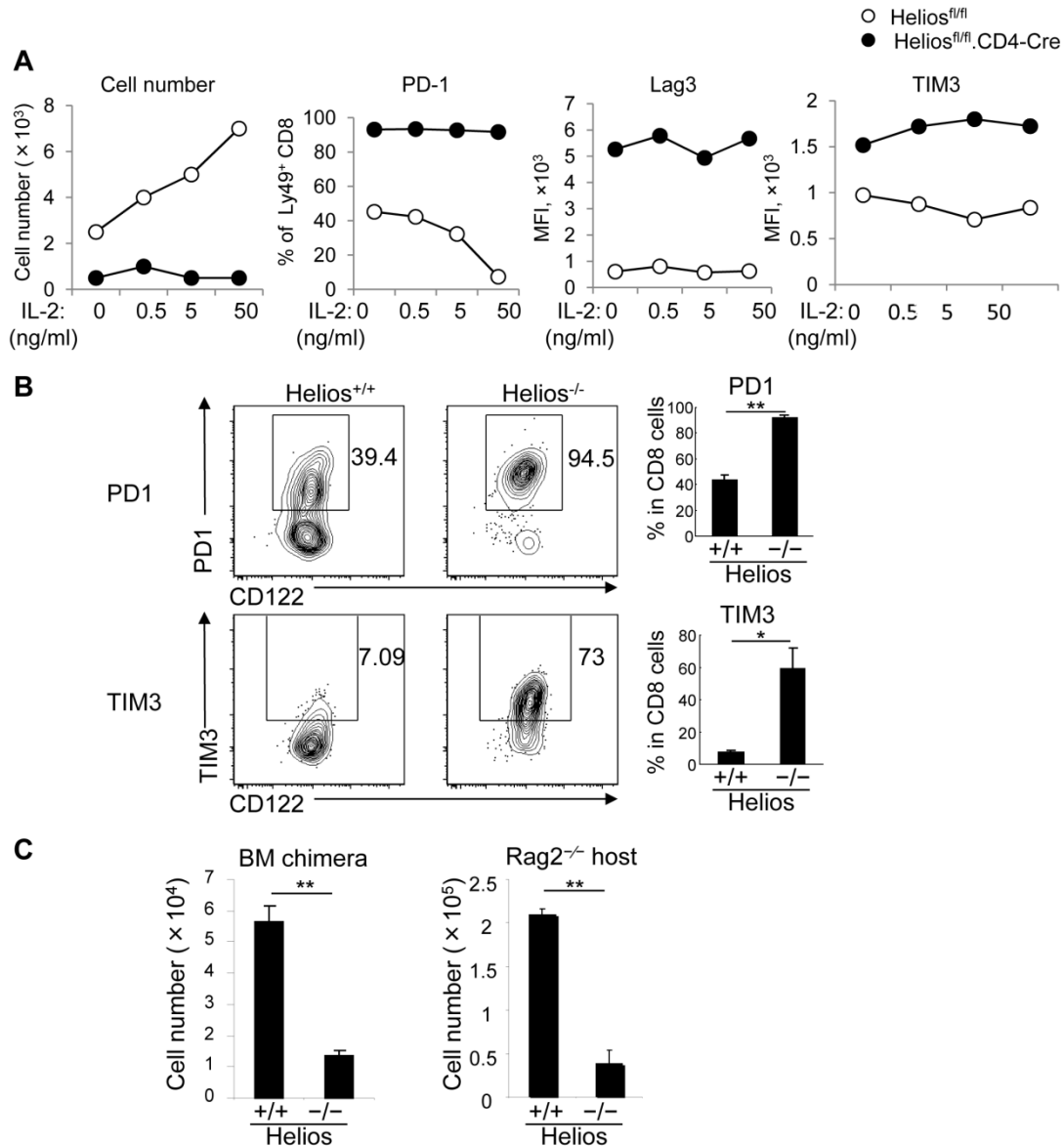


Fig. S19. Acquisition of surface phenotype characteristic of dysfunctional CD8 T cells by Helios deficient CD8 Treg exposed to inflammatory conditions.

A) Reduced IL-2 responsiveness of Helios deficient CD8 Treg. Splenic Ly49⁺ CD8 Treg were sorted from Helios^{fl/fl} or Helios^{fl/fl}.CD4-Cre mice and cultured with the supplement of different concentration of IL-2. 48 hrs later, cell numbers and surface phenotype of recovered CD8 Treg were analyzed. **B)** FACS-sorted Ly49⁺ CD8 cells (>99%) were transferred into Rag2^{-/-} hosts along with OT-II cells followed by immunization with OT-II peptides in IFA. After 12 days, CD8 T cells in spleens of these adoptive hosts were analyzed for PD-1 and TIM3 expression (n=4). The mean \pm SEM is indicated. *P < 0.05 and **P < 0.01 (Mann-Whitney test). **C)** Numbers of Ly49⁺ CD8 cells recovered from spleens of Helios^{+/+} or Helios^{-/-} BM chimeras (7 wks, Fig. 2D, S13) or Rag2^{-/-} hosts (B, above) were analyzed. All data are representative of at least two independent experiments. The mean \pm SEM is indicated. **P < 0.01 (Mann-Whitney test).

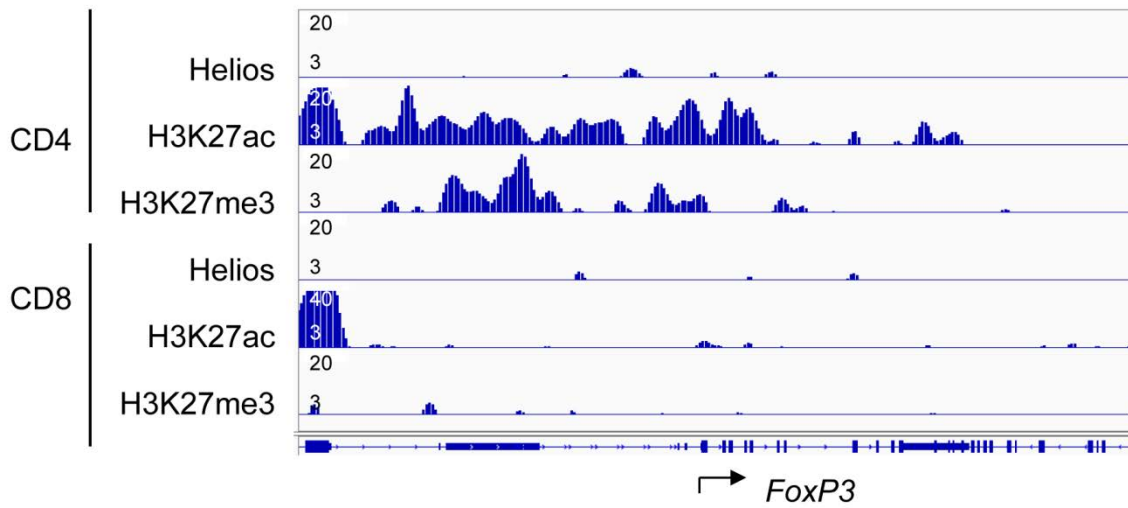


Fig. S20. Helios does not bind to the *FoxP3* locus.

Chip-Seq analysis of the binding of Helios, H3K27ac and H3K27me3 at *FoxP3* gene locus in CD4 and CD8 Treg.

Helios and Treg stability under inflammatory conditions

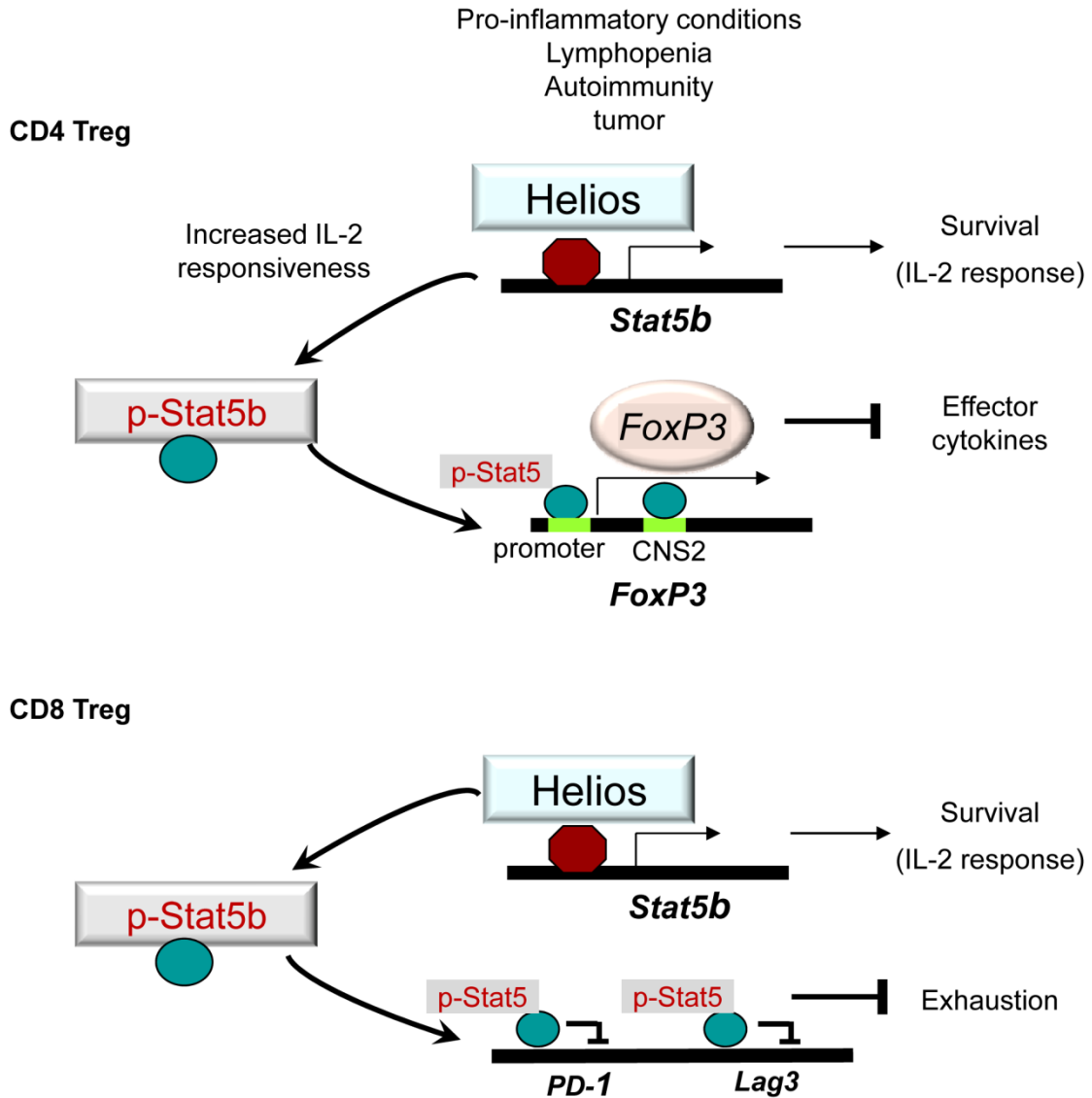


Fig. S21. Proposed mechanism of Helios-dependent Treg stability under inflammatory conditions.

Helios-dependent upregulation of genes associated with IL-2 responsiveness, including *Stat5*, increases the CD4 Treg response to IL-2, which promotes Treg stability by promoting stable *FoxP3* expression. Helios deficiency results in diminished *STAT5* activation, which in turn leads to reduced *FoxP3* expression and an unstable CD4 Treg phenotype marked by production of effector cytokines. Helios impact on *STAT5* in CD8 Treg may preempt CD8 Treg exhaustion.

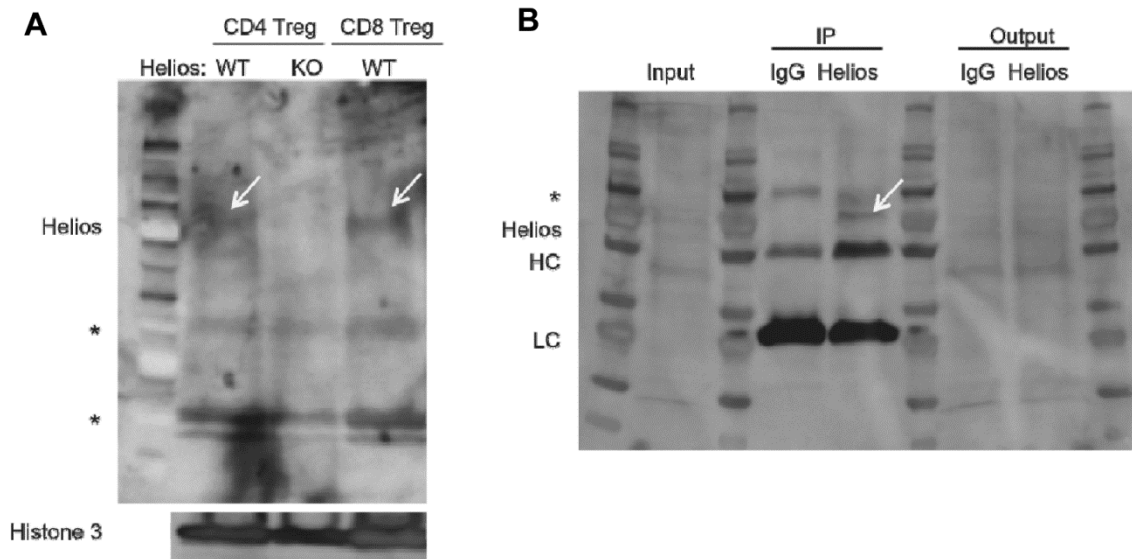


Fig. S22. Specificity of anti-Helios Ab (G-20).

CD4 and CD8 Treg isolated from Helios^{+/+} and/or Helios^{-/-} mice were activated *in vitro* by incubating with anti-CD3 and anti-CD28 Ab supplemented with IL-2 (CD4 Treg, 50 ng/ml) or IL-15 (CD8 Treg, 20 ng/ml) for 5 days. **A**) Whole cell lysates were prepared by lysing equal numbers of the indicated cells in SDS lysis buffer (60 mM Tris HCl, pH 7.2, 10% glycerol, 2% SDS) supplemented with Complete protease inhibitors (Roche) and Benzodase nuclease (Novagen). Lysates were run on a 4-20% SDS-PAGE gel (Bio-Rad) before proteins were transferred to a nitrocellulose membrane, blocked using 5% BSA in PBS with 0.1% Tween 20, and immunoblotted for Helios using anti-Helios polyclonal antibodies (G-20, Santa Cruz) and anti-goat-HRP secondary antibodies (Santa Cruz) (top blot). The arrows indicate the specific Helios bands in the WT cells but not the KO cells. Asterisks (*) indicate non-specific protein bands revealed by this Helios antibody. The membrane was immunoblotted with anti-Histone H3 polyclonal antibodies (Abcam) and anti-rabbit light chain-HRP secondary antibodies (Jackson ImmunoResearch) as a loading control. **B**) WT CD4 Treg cells were lysed in TNT buffer (50 mM Tris HCl, pH 7.2, 150 mM NaCl, 2 mM EDTA, 1 % Triton X-100, 1 % NP-40) supplemented with Complete protease inhibitors (Roche) and phosphatase inhibitor cocktail I (EMD Biosciences). A sample of the lysate was taken as the Input fraction. The lysate was split and then immunoprecipitated using anti-Helios polyclonal antibodies (G-20, Santa Cruz) or normal goat IgG (Santa Cruz). After immunoprecipitation, a sample of the unbound protein fraction was taken as the Output fraction. The Input, IP, and Output fractions were immunoblotted as in A. The only band found in the Helios IP but not the IgG IP was Helios (arrow). Cross reactivity to heavy chain (HC) and light chain (LC) of the IP antibodies was seen due to the use of the same anti-Helios antibodies for both immunoprecipitation and immunoblotting.

A Helios Targets in CD4 Treg		Helios Targets in CD8 Treg	
<u>Cell Cycle/Proliferation Gene Ontology</u>		<u>Cell Cycle/Proliferation Gene Ontology</u>	
Cell cycle	P = 2.7e-13	Cell cycle	P = 2.4e-5
Cell division	P = 2.9e-10	Cell division	P = 3.5e-5
Mitotic cell cycle	P = 1.2e-8	Chromosome organization	P = 9.6e-5
<u>Cell Death/Survival Gene Ontology</u>		<u>Cell Death/Survival Gene Ontology</u>	
Apoptosis	P = 1.0e-4	Apoptosis	P = 2.3e-2
Programmed Cell Death	P = 1.6e-4	Programmed Cell Death	P = 2.7e-2
Cell Death	P = 3.4e-4	Cell Death	P = 3.6e-2

B

CD4 Treg			CD8 Treg		
Aifm1	Dpf2	Phlda3	Aatf	Fbxo31	Ppp2ca
Atm	E2f2	Ppm1f	Apc	Fbxo5	Rad21
Bad	Eif5a	Prkdc	Arl3	Gramd4	Ran
Bag1	Ercc2	Rabep1	Bag1	Hinfp	Rassf1
Bag4	Faim	Rad21	Banp	Ilkap	Rbbp8
Bat3	Fastkd3	Rnf130	Bfar	Ints3	Rbm7
Bcl2	Gramd4	Rock1	Birc2	Lig4	Rnf130
Bfar	Il2ra	Rtn3	Ccni	Lig4	Rock1
Birc2	Jak2	Shf	Cdc7	Mapk7	Rtn3
Bnip2	Lig4	Sltm	Ctnnb1	Mapk7	Sirt7
Casp2	Luc7l3	Srgn	Dap	Mlh3	Smarcb1
Ccar1	Mapk7	Stat5b	Ddx11	Mycbp2	Smc4
Cln5	Mef2a	Tax1bp1	Dedd2	Ndufa13	Spast
Ctnnb1	Nae1	Tfdp1	Dffb	Nisch	Stag1
Dad1	Ndufa13	Tia1	Dnaja3	Nup62	Stat5
Dap	NFAT5	Tial1	Dpf2	Opa1	Stx2
Dapk3	Nisch	Tmbim6	E2f6	Pard6b	Tia1
Dedd2	Nup62	Topors	Eid1	Pds5b	Tmbim6
Dffb	Opa1	Tradd	Eif5a	Pim3	Tradd
Dido1	Pdcd5	Wwox	Esco1	Pkmyt1	Tubg1
Dnaja3	Pdcd6ip	Zc3h8	Fastkd3	Ppm1d	Wwox
	Pdcl3	Zfp346		Ppp1cb	Zfp318

Table S1. Helios target genes associated with cell cycle & survival